Supporting Information

Thiophenol-Spaced 2D Coordination Polymers with Extraordinary Alkali Resistance and Efficient Photothermal Conversion

Qin Hou[a,b], Li-Jun Chen[a,b], Jing He[b], Er-Xia Chen[b,c,d], Xuechou Zhou[e], Yumei Dai[f], Bo Wang[a,b], Liang He*[,b] and Qipu Lin*[,b,c]

[a] *College of Chemistry, Fuzhou University, Fuzhou, Fujian 350108, China*

[b] *State Key Laboratory of Structural Chemistry Fujian Institute of Research on the Structure of Matter, Chinese Academy of Sciences, Fuzhou, Fujian 350002, China*

[c] *State Key Laboratory of Photocatalysis on Energy and Environment, Fuzhou University, Fuzhou, 350116, China*

[d] *Fujian Science & Technology Innovation Laboratory for Optoelectronic Information of China, Fuzhou, Fujian 350108, China*

[e] *School of Life Sciences, Fujian Agriculture and Forestry University, Fuzhou, Fujian 350002, China*

[f] *Institute of Chemistry and Life Sciences, Minnan Science and Technolog University, Quanzhou, China*

*Corresponding Authors:heliang@fjirsm.ac.cn; linqipu@fjirsm.ac.cn

Table of Contents

Section S1: Materials and General Methods

Chemicals: All chemical reagents used are commercially available in AR grade purity and used without further purification. $Co(NO_3)_2 \cdot 6H_2O$ and N-aminoethylpiperazine (AEP) were purchased from Aladdin. $Fe(SO_4)_2 \cdot 7H_2O$, isopropyl alcohol and *N*,*N*-dimethylformamide (DMF) were purchased from Sinopharm. $ZnCl_2$ was purchased from Energy Chemical. 4,4'-thiodibenzenethiol and 1,8-diazabicyclo[5.4.0]undec-7-ene was purchased from MERYER. 4-(2-aminoethyl)morpholine was purchased from MACKLIN. 1-butyl-2,3-dimethylimidazolium chloride (BMMImCl) was purchased from Lanzhou Greenchem.

Instrumentation: Powder X-ray diffraction (PXRD) patterns was measured on a Rigaku Dmax 2500 XRD with Cu-*Kα* radiation (λ = 1.54056 Å). Elemental analyses (EA) were carried out on a Vario EL-Cube. Fourier transform infrared (FT-IR) spectra was obtained using KBr pellets on a Nicolet Magna 750 FT-IR spectrometer over a range 400~4000 cm^{-1}. Thermal analysis (TGA) was performed using a Netzsch STA449C thermal analyzer under N_2 atmosphere at a temperature range of 25 to 800 °C with a heating rate of 10 °C min^{-1}. UV–Vis diffuse reflection spectroscopy (DRS) was performed on a PerkinElmer Lamda-950 UV spectrophotometer from 250 to 900 nm using $BaSO_4$ as nonabsorbing background with 100% reflectance. X-ray photoelectron spectroscopy (XPS) was performed on ESCALAB 250Xi. The I-V curves were measured on a Keithley 4200 SCS semiconductor characterization system. The Photothermal conversion experiments were performed using a MW-GX-808/2000 mW.

Section S2: Synthetic Procedures

Synthesis of compound FeTBT: $FeSO_4 \cdot 7H_2O$ (64.5 mg 0.232 mmol), 4,4'-thiodibenzenethiol (H_2TBT) (37.5 mg, 0.15mmol), [BMMIm]Cl (500.0 mg, 2.65 mmol), DMF (1mL), isopropyl alcohol (0.5 mL), H_2O (0.5 mL) and 4-(2-aminoethyl)morpholine (0.5 mL) were mixed in a 20 mL glass bottle and ultrasonicated for 30 minutes until completely dissolved, then heated to 100 °C for 7 days. The reaction mixture was naturally cooled to room temperature, washed several times with ethanol, and brown octahedral crystals were collected with the yield of 76% based on $FeSO_4 \cdot 7H_2O$. Calculated EA date: C 58.66%, N 6.58%, H 5.82%; experimental EA data: C 57.79%, N 6.42%, H 5.53%.

Synthesis of compound CoTBT: CoTBT was synthesized by substituting $FeSO_4 \cdot 7H_2O$ and 4-(2-aminoethyl)morpholine (0.5 mL) with $Co(NO_3)_2 \cdot 6H_2O$ (45.5 mg, 0.156mmol) and N-aminoethylpiperazine (0.5 mL) in the above synthetic procedure for FeTBT. After cooling to room temperature and washing with ethanol several times, green octahedral crystals were obtained with the yield of 75% based on $Co(NO_3)_2 \cdot 6H_2O$. Calculated EA date: C 58.45%, H 5.79%, N 6.49%; experimental EA data: C 57.31%, H 5.84%, N 6.28%.

Synthesis of compound ZnTBT: ZnTBT was synthesized according to the synthetic procedure of FeTBT, but $ZnCl_2$ (53.5 mg, 0.39 mmol) and 1,8-diazabicyclo[5.4.0]undec-7-ene (0.5 mL) were added instead of $FeSO_4 \cdot 6H_2O$, DMF, 4-(2-aminoethyl)morpholine and isopropanol. After cooling to room temperature and washing with ethanol several times, colorless octahedral crystals were collected with the yield of 68% based on $ZnCl_2$. Calculated EA date: C 57.75%, N 6.41%, H 5.72%; experimental EA data: C 56.81%, H 5.51%, N 6.13%.

Section S3: Crystallographic Data

Single crystals of MTBT (M = Fe, Co and Zn) were carefully picked under an optical microscope and glued to a loop. The structures of the compounds were collected by a Synergy Custom (Liquid MetalJet D2^{+}) with Ga radiation. The diffraction images were reduced with Crystalclear software and their empirical absorption corrections were treated with the CrysAlisPro software. The structures were solved by the direct methods, and the full-matrix least-squares refinements of F^2 were performed using the SHELXL program package.[1] All the nonhydrogen atoms were anisotropically refined and their positions were fixed at calculated positions and isotropically refined.

(a)

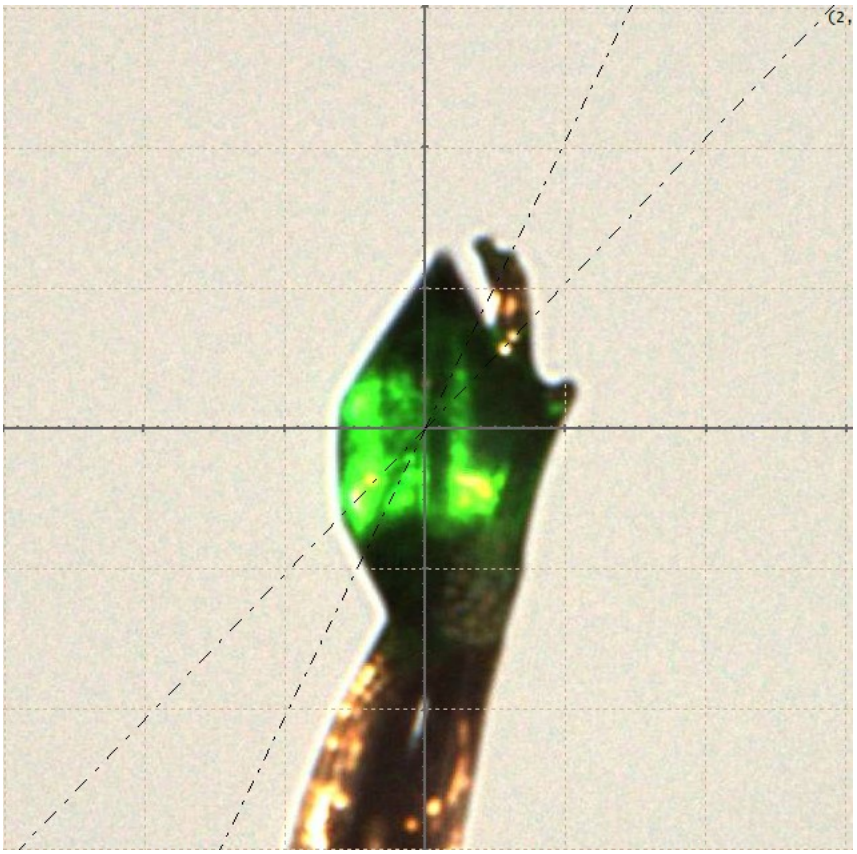

(b)

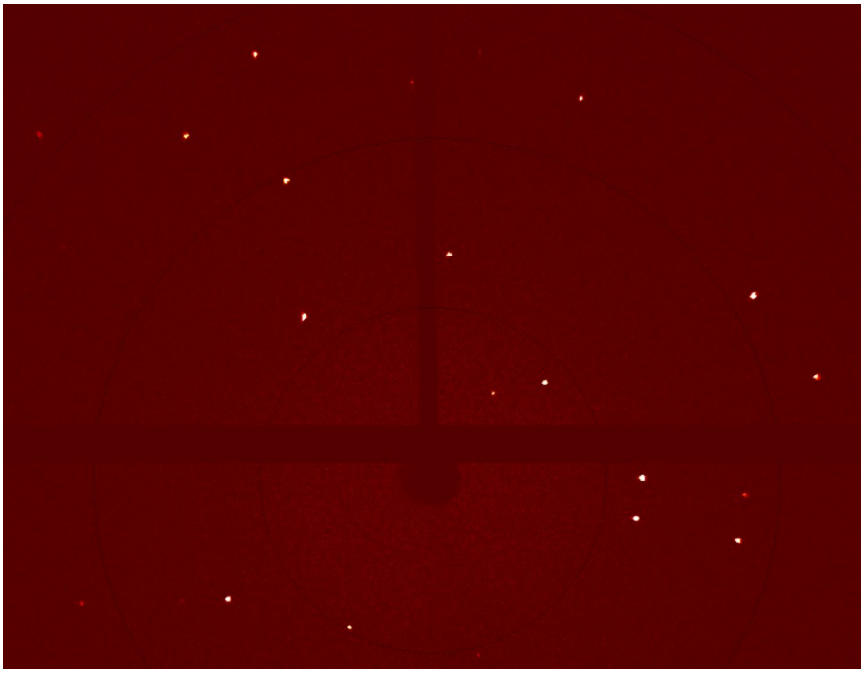

Figure S1. (a) Determination of the lattice planes of CoTBT. (b) Single-crystal XRD image of CoTBT.

Table S1 Crystallographic data and structural refinements for MTBT (M = Fe, Co and Zn). CCDC 2242745, 2242746 and 2242747.

Compound	FeTBT	CoTBT	ZnTBT
Chemical formula	$C_{42}H_{50}N_4S_6Fe$	$C_{42}H_{50}N_4S_6Co$	$C_{42}H_{50}N_4S_6Zn$
F.W.	859.07	862.22	872.62
Space group	$P2_1/n$	$P2_1/n$	$I4_1/a$
a(Å)	16.9805(8)	16.9834(3)	11.35023(6)
b(Å)	16.3895(5)	16.3415(2)	11.35023(6)
c(Å)	17.0828(8)	17.0437(3)	34.2177(3)
α(°)	90	90	90
β(°)	116.751(6)	116.574(3)	90
γ(°)	90	90	90
$V(Å^3)$	4245.3(4)	4230.50(16)	4408.19 (6)
Z	4	4	4
D_{calcd} (g cm^{-3})	1.344	1.354	1.315
Temp. (*K*)	100	100	200
μ(mm^{-1})	0.69	0.74	2.43
F(000)	1808.0	1816.8299	1840
Reflections collected	61423	62691	29764
GOF on F^2	1.082	1.052	1.093
[a]R_1, wR_2 ($I > 2\sigma$ (I))	0.0341/0.0840	0.0341/0.0763	0.0529/0.166844
[b]R_1, wR_2 (all data)	0.0386/0.0857	0.0379/0.0779	0.0565/0.1722

[a]$R_1 = \sum||Fo| - |Fo||/\sum|Fo|$. [b]$wR_2 = [\sum w(Fo^2 - Fc^2)^2/\sum w(Fo^2)^2]^{1/2}$

Section S4: Additional Structural Figures

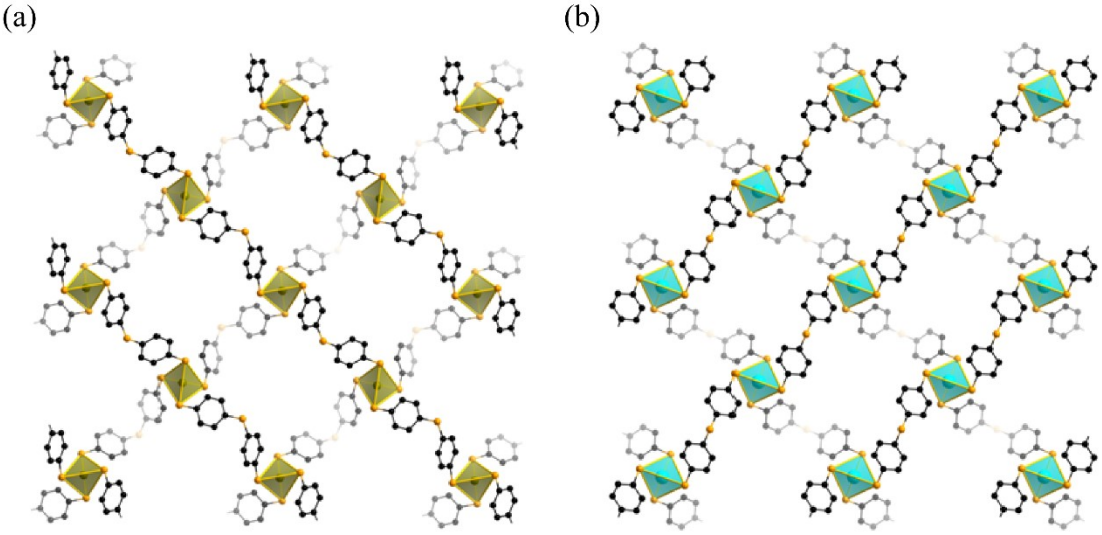

Figure S2. 2D $[Fe/Co\ (TBT)_2]_n^{2n-}$ (a) and $[Zn\ (TBT)_2]_n^{2n-}$ (b) anionic layers.

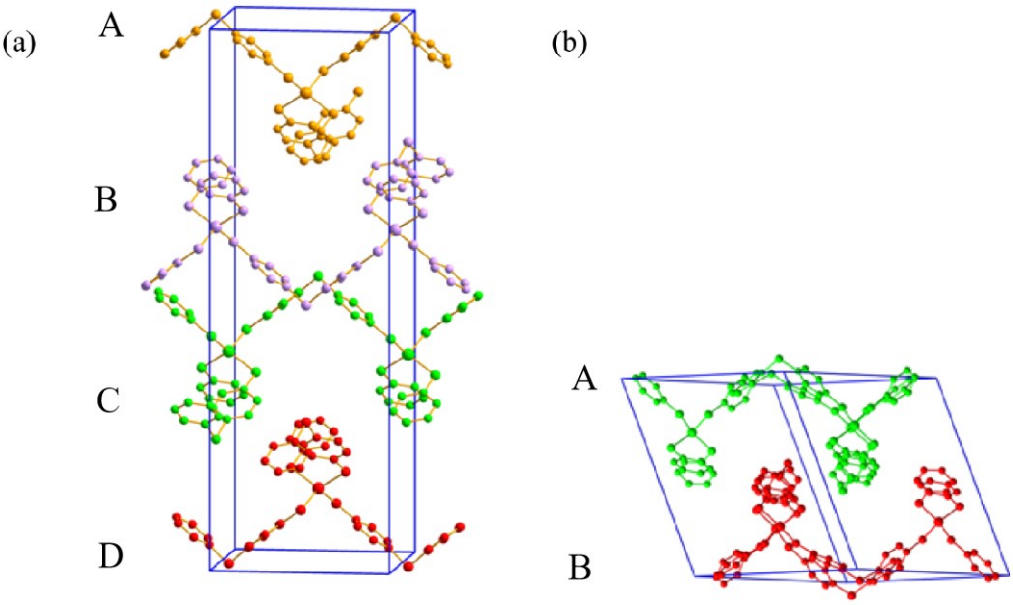

Figure S3. The packing diagrams of ZnTBT (a) and Fe/CoTBT (b).

In ZnTBT, layers B and C exhibit visually partially interleaved but not interpenetrate, which can be attributed to the bending configuration of the flexible ligand, 4,4'-thiobisbenzenethiol.

Section S5: FT-IR/ UV-Vis DRS

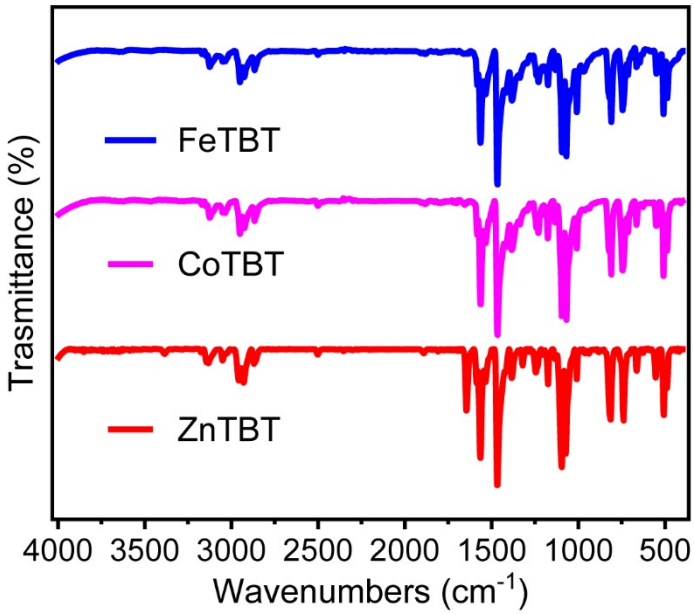

Figure S4. FT-IR spectra of MTBT (M = Fe, Co and Zn).

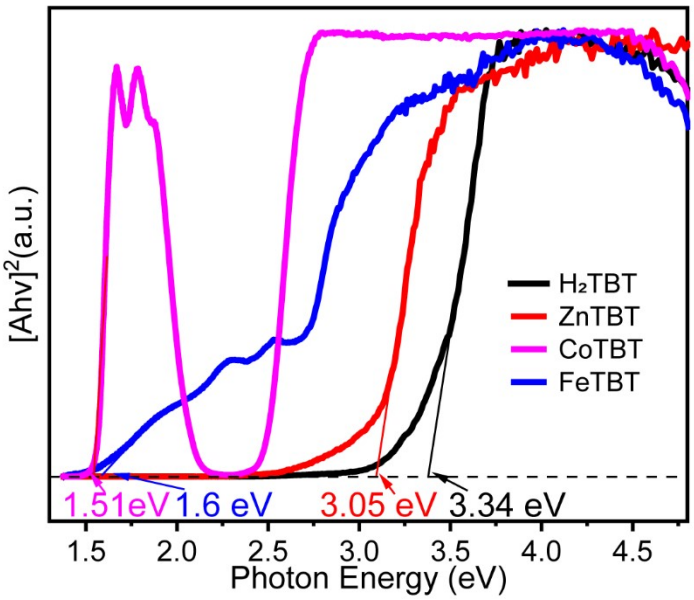

Figure S5. Tauc plots of MTBT (M = Fe, Co and Zn) derived from solid-state UV-Vis DRS.

Section S6: Conductivity Experiments

The I-V curves of MTBT (M = Fe, Co and Zn) powder pellets were obtained using a semiconductor analysis system (Keithley 4200). Firstly, 6 mg of MTBT was pressed into cylindrical pellet at a pressure of 0.25 GPa with a diameter of 0.25 cm and a thickness of 0.062 cm for M = Fe and Co, 0.064 cm for M = Zn, respectively. Then, the round surfaces of the pellets were covered by silver conductive paint and connected to the 4200 analyzers via gold wires with a diameter of 50 μm. The voltage scan ranges from □5 to 5 V with a scanning step of 0.2 V. To obtain the E_a, the I-V curves of MTBT crystals were tested in the temperature range from 50 to 120 °C with a step of 10 °C.

(a)

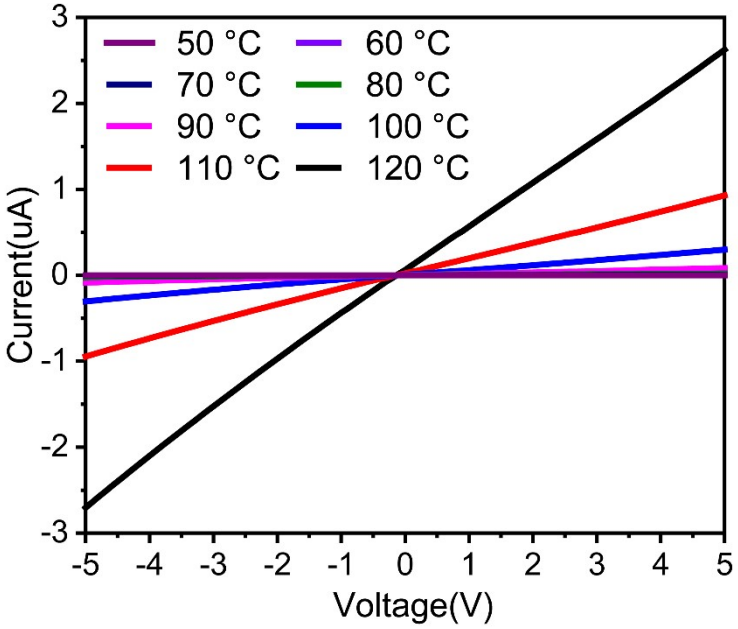

(b)

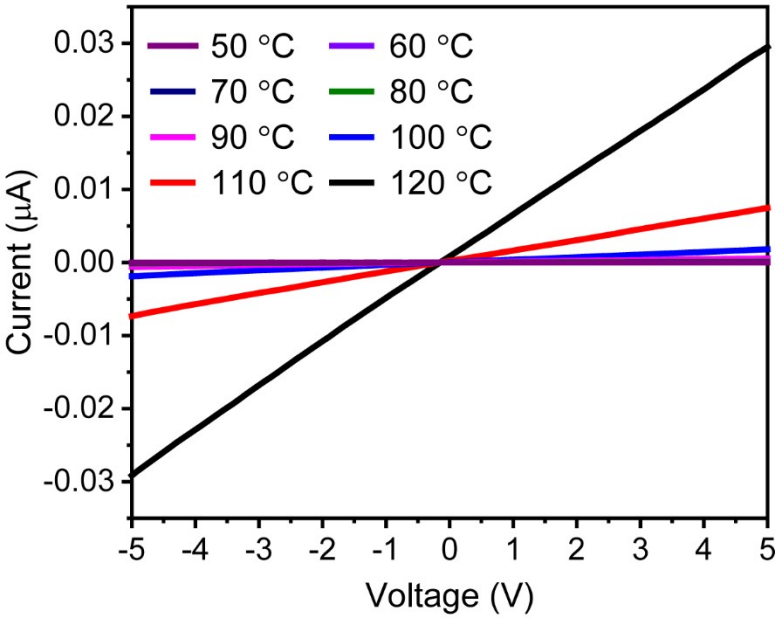

Figure S6. Temperature-dependent I–V curves of FeTBT (a) and ZnTBT (b).

Section S7: X-ray Photoelectron Spectroscopy (XPS)

XPS was used to investigate the chemical valence states of elements in the sample. As shown in Figure S7, there are S, N, O and C in the FeTBT and CoTBT. The high resolution XPS for Fe 2p (Figure 4e) are similar to the results found in the literatures.[2] The peaks at 710.6 and 723.64 eV are attributed to the Fe^{2+}states, whereas the 712.71 and 726.71 eV peaks are attributed to the Fe^{3+} states, confirming the coexistence of Fe^{2+}/Fe^{3+} states. The peak at 718.67 eV is corresponding to the satellite peak, which could be attributed to the surface oxidation of the sample in the air. The high resolution XPS for Co 2p (Figure 4e) with the satellite peaks at 786.29 and 802.52 eV. The peaks at 795.4 and 779.54 eV are attributed to the Co^{2+}states, whereas the 798.98 and 782.62 eV peaks are attributed to the Co^{3+} states, also confirming the coexistence of Co^{2+}/Co^{3+} states.[3]

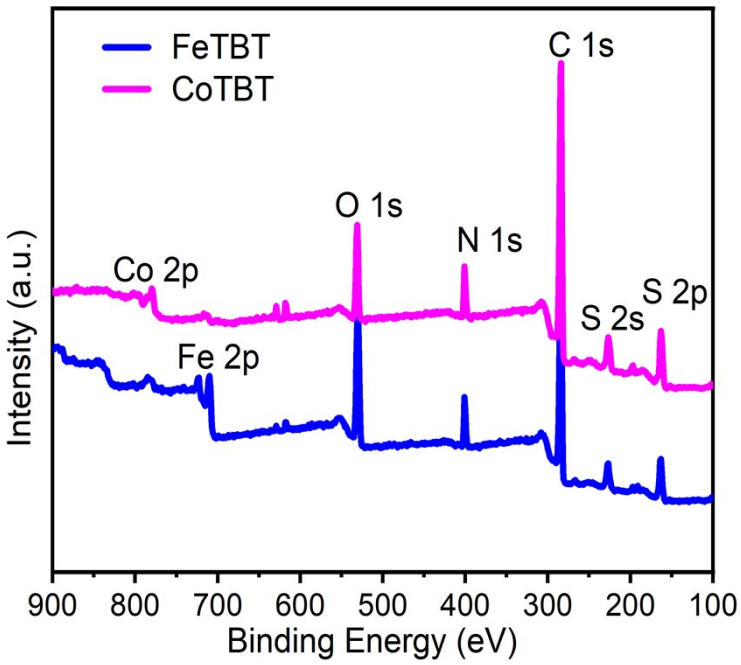

Figure S7. XPS spectra of FeTBT and CoTBT.

Section S8: Stability Analysis

(a)

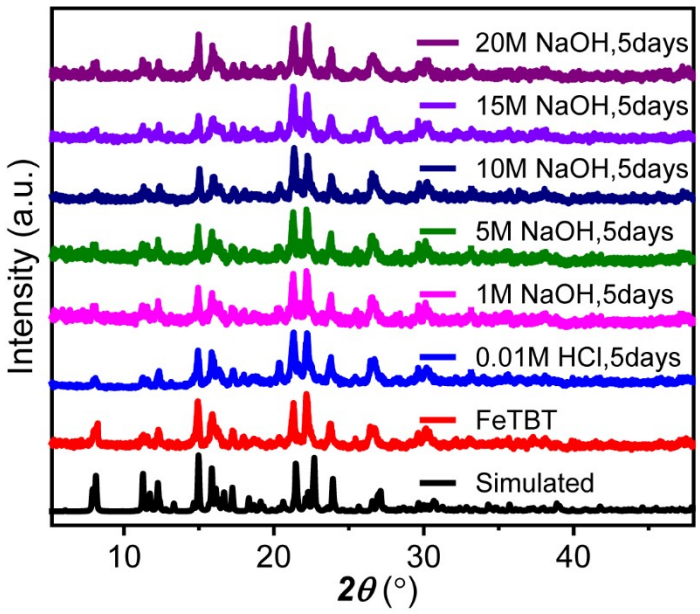

(b)

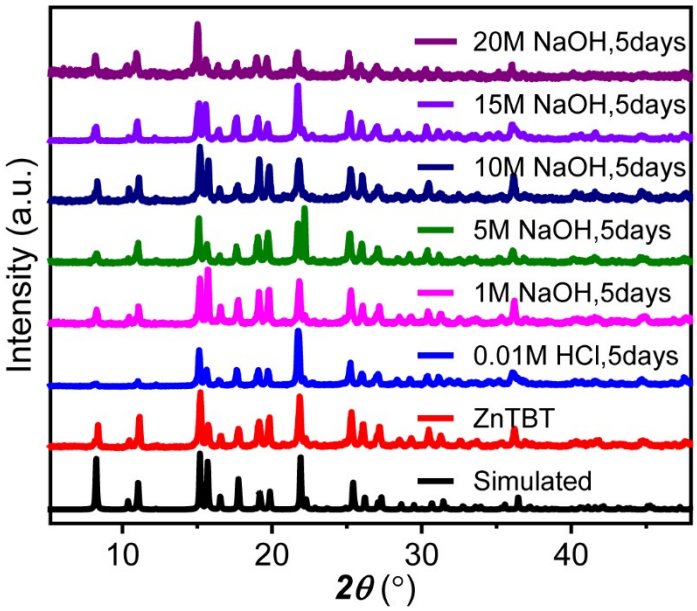

Figure S8. PXRD patterns of FeTBT (a) and ZnTBT (b) after immersion in aqueous solutions of 0.01M HCl to 20M NaOH for 5 days at room temperature.

(a)

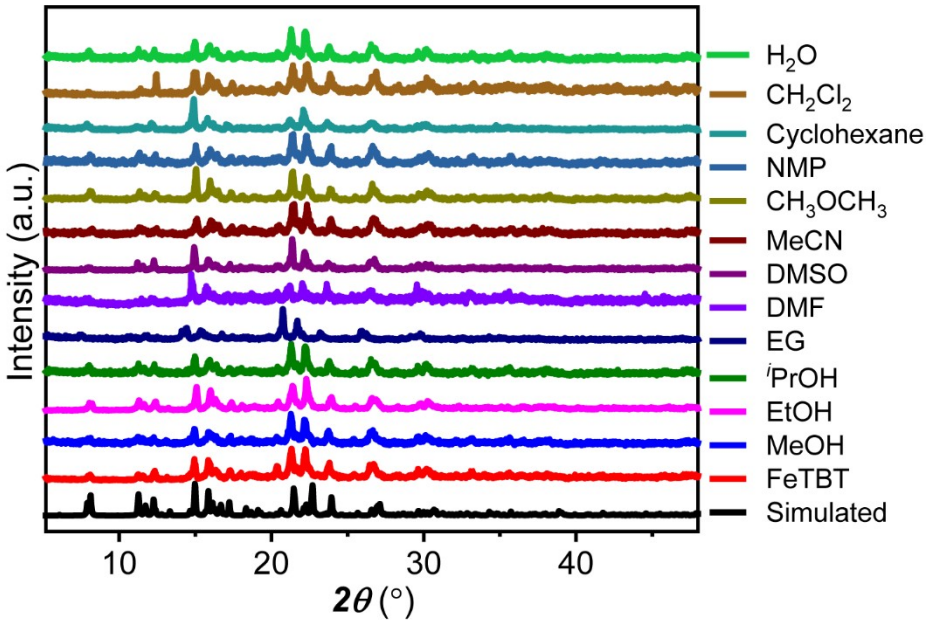

(b)

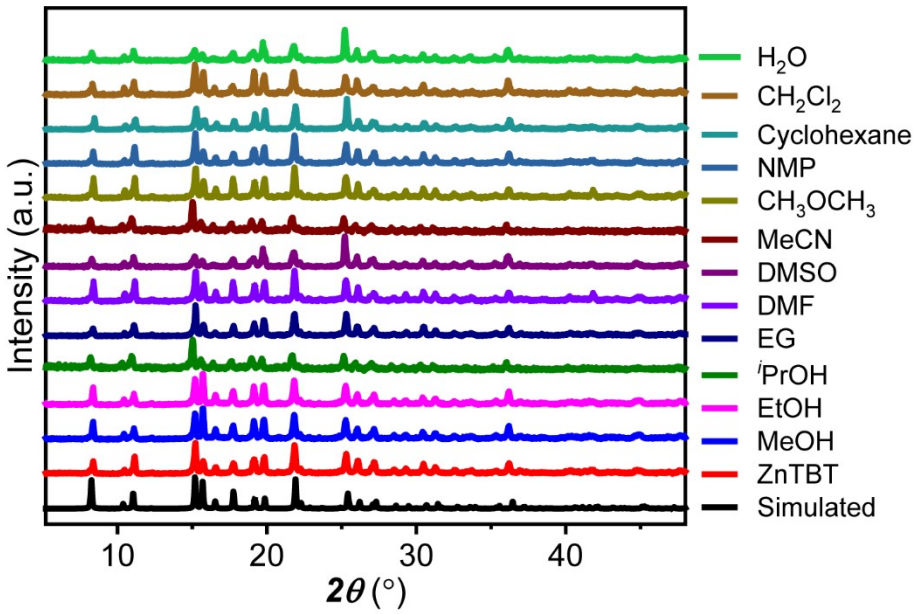

Figure S9. PXRD patterns of FeTBT (a) and ZnTBT (b) after immersion in different solutions for 7 days at room temperature.

Figure S10. Photograph of the compound CoTBT after immersion in 20M NaOH for 5 days at room temperature.

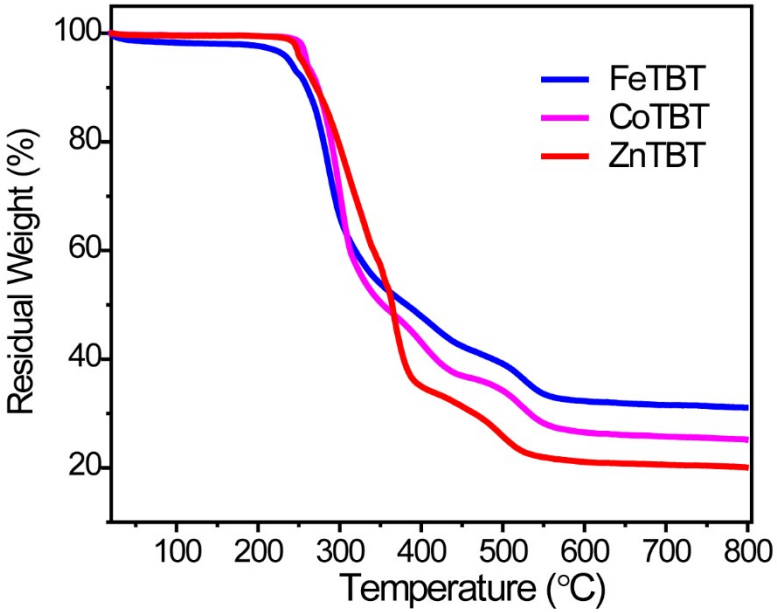

Figure S11. TGA curves of MTBT (M = Fe, Co and Zn) in the N_2 atmosphere.

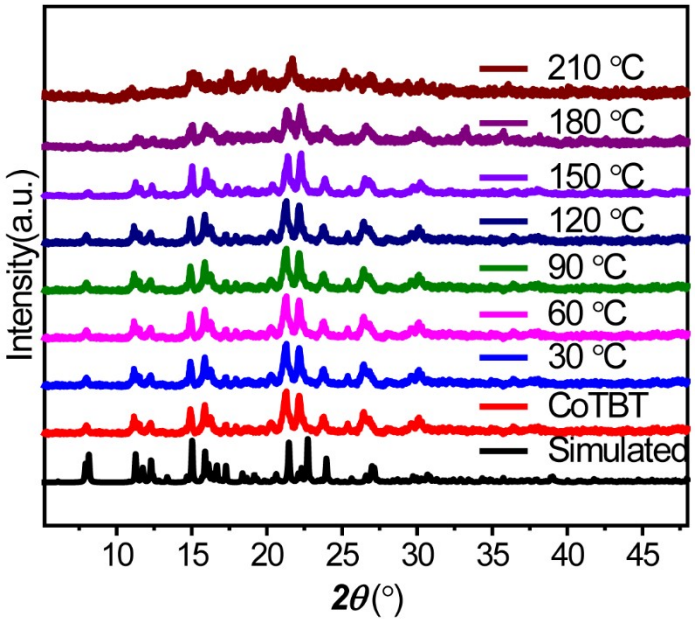

Figure S12. The PXRD patterns of CoTBT under different temperatures in the air atmosphere.

Section S9: Photothermal Conversion Experiments

The crystals of MTBT (M = Fe, Co and Zn) and the ligand H_2TBT with a mass of 5 mg were pressed into a thin pellet with a diameter of 0.5 cm spread on a quartz slide above which an 808 nm laser (MW-GX-808/2000 mW) was set at a distance of 8 cm. The power density of laser was varied from 0.1 to 0.5 W cm^{-2} with a step of 0.1 W cm^{-2}. An IR thermal camera is used to timely record the temperature changes under laser irradiation.

(b)

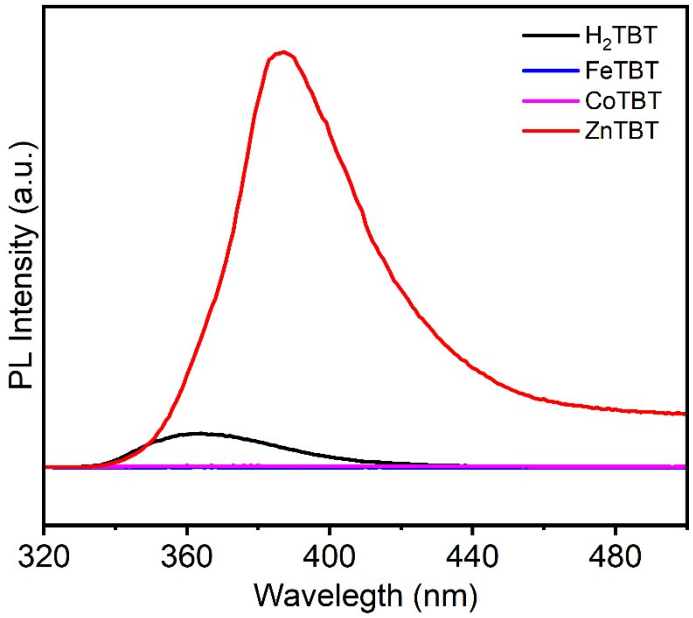

Figure S13. The PL emission spectra of MTBT (M = Fe, Co and Zn) and H_2TBT (λex = 300 nm).

(a)

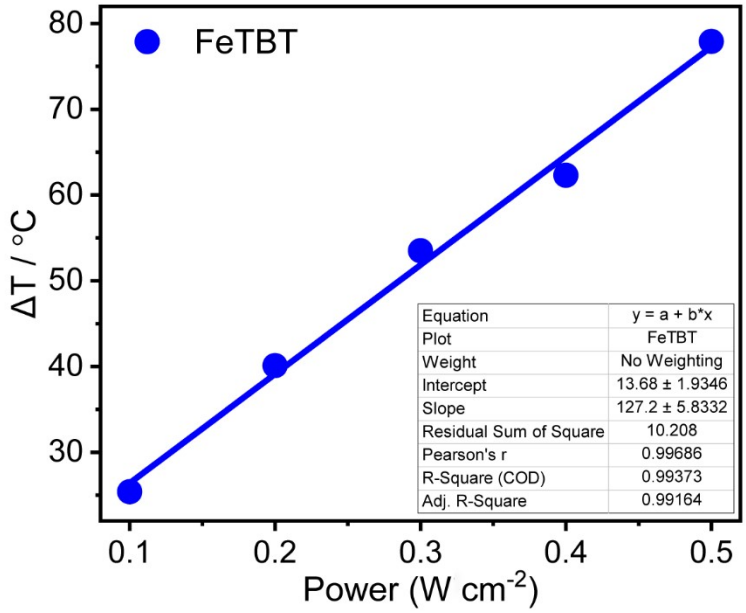

(b)

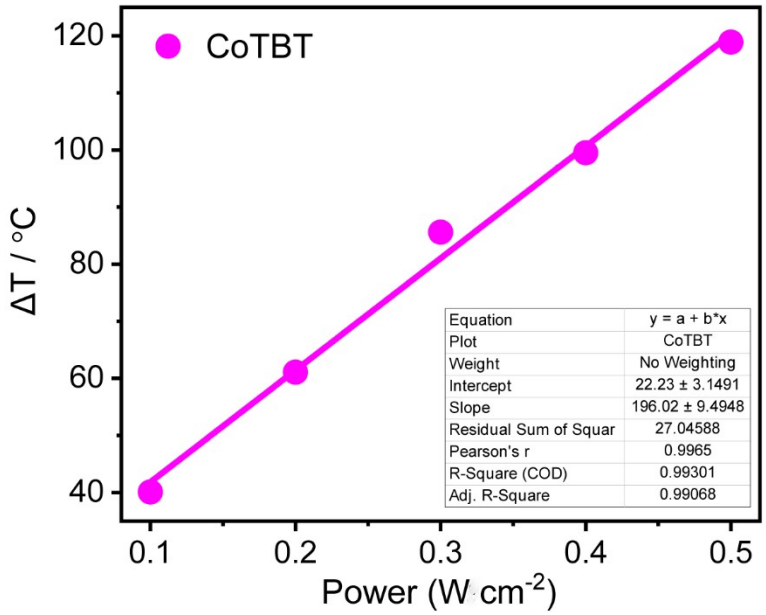

Figure S14. Plots of average temperature rise (ΔT) against power density of 808 nm laser for FeTBT (a) and CoTBT (b).

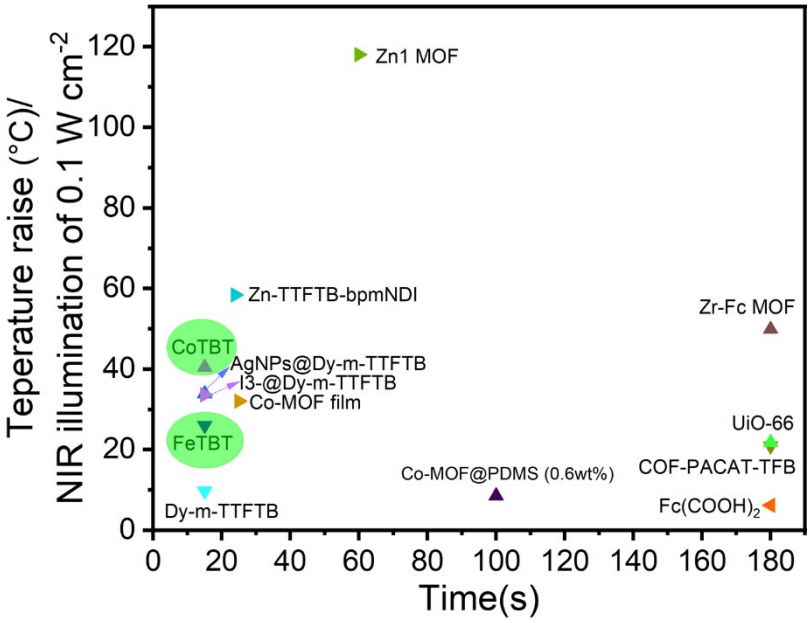

Figure S15. The temperature increases of photothermal materials irradiated by 808 nm laser (0.1 W cm^{-2}) in the literatures.

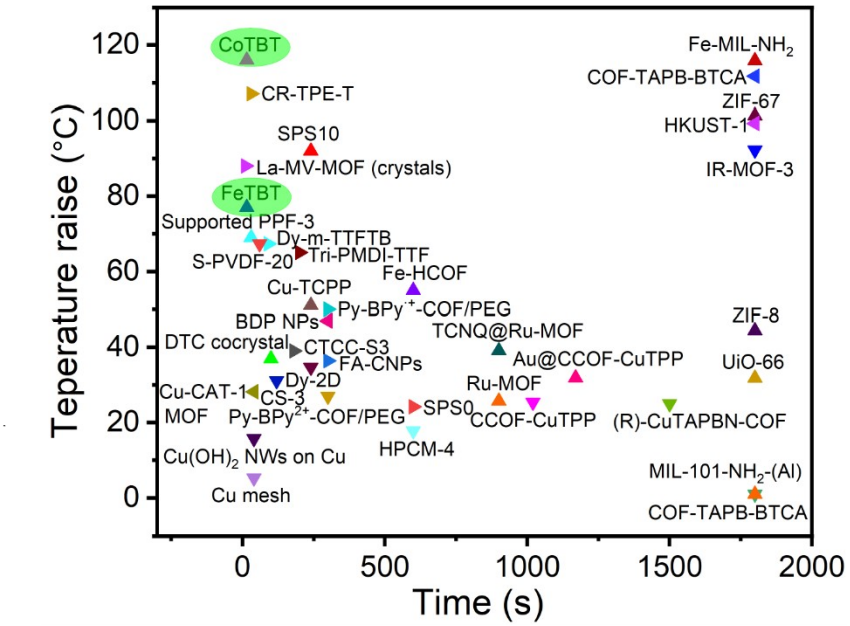

Figure S16. The temperature changes for various solid-state photothermal materials reported in the references.

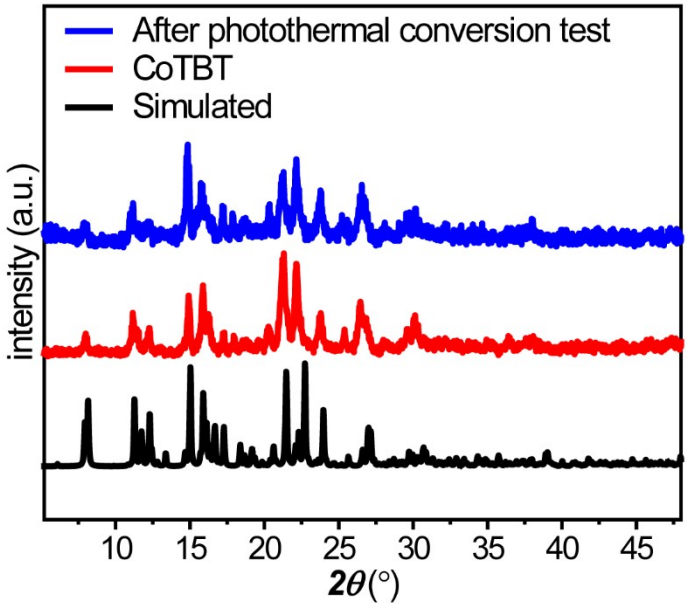

Figure S17 PXRD patterns of CoTBT before and after photothermal conversion testing.

Table S2. Photothermal conversion efficiency of the various solid-state materials triggered by 808 nm NIR in the references (the Ag-2D-CPs NIR light source is 800 nm).

Samples	Light Intensity	Temperature ranges	Added temperature	Pretreatmnt	Ref.
FeTBT	0.1 W cm^{-2}	19.6-45.6 °C	26 °C in 15 s	None	This work
	0.5 W cm^{-2}	19.2-96.5 °C	77 °C in 15 s		
CoTBT	0.1 W cm^{-2}	19.2-59.6 °C	40.4 °C in 15 s		
	0.5 W cm^{-2}	19.2-135.2 °C	116 °C in 15 s		
		19.2-141.8 °C	122.6 °C in 36 s		
AgNPs@Dy-m-TTFTB	0.1 W cm^{-2}	21.3-55.2°C	33.9 °C in 15 s	None	4
	0.5 W cm^{-2}	21.3-156.4 °C	135.1 °C in 15 s		
Dy-m-TTFTB	0.1 W cm^{-2}	21.3-31 °C	9.7 °C in 15 s		
	0.5 W cm^{-2}	21.3-65.2°C	43.9 °C in 15 s	None	
I3-@Dy-m-TTFTB	0.1 W cm^{-2}	21.3-54.9 °C	33.6 °C in 15 s		
	0.5 W cm^{-2}	21.3-145.8 °C	124.5 °C in 15 s		
Co-MOF film	0.1 W cm^{-2}	22-55 °C	32 °C in 25 s	None	5
	0.5 W cm^{-2}	22-156.5 °C	134.5 °C in 25 s		
Co-MOF@PDMS (0.6wt%)	0.1 W cm^{-2}	20-28.58 °C	8.58 °C in 100 s		
	0.5 W cm^{-2}	20-62 °C	42°C in 100 s		
Ag-2D-CPs	0.1 W cm^{-2}	-	24.5 °C in 180 s	None	6
Zr-$PDI^{\bullet-}$ film	0.5 W cm^{-2}	25-95 °C	70 °C in 100 s	TEA vapor fumigation Blue light Irradiation.	7
Zn-MOF	0.1 W cm^{-2}	25-104 °C	79 °C in 24 s	None	8
Zr-Fc MOF	0.1 W cm^{-2}	25-74.9 °C	49.9 °C in 180 s	None	9
	0.5 W cm^{-2}	25-92 °C	67 °C in 18 0 s		
$Fc(COOH)_2$	0.1 W cm^{-2}	25-31.2 °C	6.2 °C in 180 s		
UiO-66	0.1 W cm^{-2}	25-46.8 °C	21.8 °C in 180 s		
COF-PACAT-TFB	0.5 W cm^{-2}	26-46.9 °C	20.9 °C in 180 s	None	10
MV-based MOF film	0.5 W cm^{-2}	23-40 °C	17 °C in 200 s	None	11
Zn1 MOF	0.1 W cm^{-2}	25-143 °C	118 °C in 60 s	None	12
Cu2O/Zr-Fc-MOF composite	0.5 W cm^{-2}	28-32 °C	4 °C in 600 s	None	13
Fe-NDC	0.5 W cm^{-2}	22.5-67.8 °C	45.3 °C in 100 s	None	14
Co-NDC	0.5 W cm^{-2}	22.4-57.7 °C	35.3 °C in100 s		

Table S3. The photothermal properties in this work compared with previous results of solid-state materials in the references.

Samples	Light source	Light Intensity	Temperature ranges	Added temperature	Ref.
FeTBT	808 nm NIR laser	0.5 W cm^{-2}	19.2-96.5 °C	77 °C in 15 s	This work
CoTBT	808 nm NIR laser	0.5 W cm^{-2}	19.2-135.2 °C	116 °C in 15 s	
Fe-MIL-NH_2	UV-Vis irradiation (300-650 nm)	0.5 W cm^{-2}	27.6-143.4 °C	115.8 °C in 30 min	15
COF-TAPB-BTCA	UV-Vis irradiation (300-650 nm)	0.5 W cm^{-2}	26.6-141.4 °C	114.8 °C in 30 min	15
CPO-27-Mg	UV-Vis irradiation (300-650 nm)	0.5 W cm^{-2}	24.1-135.8 °C	111.7 °C in 30 min	15
CR-TPE-T	808 nm NIR laser	1.2 W cm^{-2}	22-129 °C	107 °C in 30 s	16
ZIF-67	UV-Vis irradiation (300-650 nm)	0.5 W cm^{-2}	26.4-127.7 °C	101.3 °C in 30 min	15
HKUST-1	UV-Vis irradiation (300-650 nm)	0.5 W cm^{-2}	25.0-124.7 °C	99.3 °C in 30 min	15
IR-MOF-3	UV-Vis irradiation (300-650 nm)	0.5 W cm^{-2}	26.4-118.6 °C	92.2 °C in 30 min	15
SPS10	visible light	0.241 W cm^{-2}	-	92 °C in 4 min	17
La-MV-MOF (crystals)	808 nm NIR laser	2 W cm^{-2}	23.1-111.1 °C	88 °C in 10 s	11
Supported PPF-3	Xe lamp	0.1 W cm^{-2}	20-89 °C	69 °C in 30 s	18
Dy-m-TTFTB	808 nm NIR laser	0.7 W cm^{-2}	22.8-90.1 °C	67.3 °C in 90 s	4
S-PVDF-20	50 W ultraviolet lamp (400 nm)	-	25-92.3 °C	67.3 °C in 60 s	19
Tri-PMDI-TTF	808 nm NIR laser	0.7 W cm^{-2}	15-80 °C	65 °C in 200 s	20
Fe-HCOF	808 nm NIR laser	1.8 W cm^{-2}	19-74 °C	55 °C in 10 min	21
Py-$BPy^{\cdot+}$-COF/PEG	808 nm NIR laser	1 W cm^{-2}	25-75 °C	50 °C in 5 min	22
Py-BPy^{2+}-	808 nm NIR laser	1 W cm^{-2}	25-52 °C	27 °C in 5 min	22

COF/PEG					
Cu-TCPP	visible light	0.241 W cm^{-2}	-	51 °C in 4 min	17
BDP NPs	808 nm NIR laser	0.32 W cm^{-2}	27-74 °C	47 °C in 5 min	23
MIL-101-NH2-(Al)	UV-Vis irradiation (300-650 nm)	0.5 W cm^{-2}	24-70 °C	46 °C in 30 min	24
ZIF-8	UV-Vis irradiation (300-650 nm)	0.5 W cm^{-2}	26.1-70.5 °C	44.4 °C in 30 min	15
TCNQ@Ru-MOF	980 nm laser	-	26-65.1 °C	39.1 °C in 15 min	25
CTCC-S3	1 sun light	0.1 W cm^{-2}	21.1-60.1 °C	39 °C in 3 min	26
DTC cocrystal	800 nm NIR laser	0.7 W cm^{-2}	29-66 °C	37 °C in 100 s	27
FA-CNPs	808 nm NIR laser	0.7 W cm^{-2}	23.6-60 °C	36.4 °C in 5 min	28
Dy-2D	1 sun light	0.1 W cm^{-2}	29.2-63.9 °C	34.7 °C in 4 min	29
Au@CCOF-CuTPP	300W xenon lamp $\lambda > 400$ nm	2.5 W cm^{-2}	-	31.9 °C in 19.5 min	30
UiO-66	UV-Vis irradiation (300-650 nm)	0.5 W cm^{-2}	25.5-57.3 °C	31.8 °C in 30 min	15
CS-3	1 sun light	0.1 W cm^{-2}	25-56.1 °C	31.1 °C in120 s	31
Cu-CAT-1 MOF	1 sun light	0.1 W cm^{-2}	25-53.2 °C	28.2 °C in 40 s	32
Ru-MOF	980 nm laser	-	26-51.7 °C	25.7 °C in 15 min	25
CCOF-CuTPP	300Wxenon lamp $\lambda > 400$ nm	2.5 W cm^{-2}	-	25.4 °C in 17 min	30
Pd@CCOF-CuTPP	300Wxenon lamp $\lambda > 400$ nm	2.5 W cm^{-2}	-	25.3 °C in 18 min	30
(R)-CuTAPBN-COF	visible light λ = 420 nm	2.5 W cm^{-2}	25-50 °C	25 °C in 18min	33
SPS0	visible light	0.241 W cm^{-2}	-	24.2 °C in 10 min	17
HPCM-4	1 sun light	0.1 W cm^{-2}	24-41.2 °C	17.8 °C in 60 min	34
$Cu(OH)_2$ NWs on Cu	1 sun light	0.1 W cm^{-2}	25-40.7 °C	15.7 °C in 40 s	32
Cu mesh	1 sun light	0.1 W cm^{-2}	25-30.3 °C	5.3 °C in 40 s	32

S10: References

1. O. V. Dolomanov, L. J. Bourhis, R. J. Gildea, J. A. K. Howard and H. Puschmann, *J. Appl. Crystallogr.*, 2009, **42**, 339-341.
2. D. Li, Y. Sun, S. Chen, J. Yao, Y. Zhang, Y. Xia and D. Yang, *ACS Appl. Mater. Interfaces*, 2018, **10**, 17175-17182.
3. (a) W. Liu, E. Hu, H. Jiang, Y. Xiang, Z. Weng, M. Li, Q. Fan, X. Yu, E. I. Altman and H. Wang, *Nat. Commun.*, 2016, **7**, 10771; (b) F. T. Haase, A. Rabe, F.-P. Schmidt, A. Herzog, H. S. Jeon, W. Frandsen, P. V. Narangoda, I. Spanos, K. Friedel Ortega and J. Timoshenko, *J. Am. Chem. Soc.*, 2022, **144**, 12007-12019.
4. J. Su, P. Cai, T. Yan, Z.-M. Yang, S. Yuan, J.-L. Zuo and H.-C. Zhou, *Chem. Sci.*, 2022, **13**, 1657-1664.
5. T. Yan, Y. Y. Li, J. Su, H. Y. Wang and J. L. Zuo, *Chem. Eur. J.*, 2021, **27**, 11050-11055.
6. M.-Q. Li, M. Zhao, L.-Y. Bi, Y.-Q. Hu, G. Gou, J. Li and Y.-Z. Zheng, *Inorg. Chem.*, 2019, **58**, 6601-6608.
7. B. Lü, Y. Chen, P. Li, B. Wang, K. Müllen and M. Yin, *Nat. Commun.*, 2019, **10**, 767.
8. T. Yan, Y.-Y. Li, Q.-Y. Gu, J. Li, J. Su, H.-Y. Wang and J.-L. Zuo, *Inorg. Chem.*, 2022, **61**, 3078-3085.
9. Z. Deng, C. Fang, X. Ma, X. Li, Y.-J. Zeng and X. Peng, *ACS Appl. Mater. Interfaces*, 2020, **12**, 20321-20330.
10. X. Q. Xu, Z. Wang, R. Li, Y. He and Y. Wang, *Chem. Eur. J.*, 2018, **24**, 9769-9772.
11. S. Wang, S. Li, J. Xiong, Z. Lin, W. Wei and Y. Xu, *Chem. Commun.*, 2020, **56**, 7399-7402.
12. Q. Gu, Z.-H. Zhao, B. Chan, T. Yan, J.-L. Zuo, D. M. D'Alessandro and C.-H. Li, *ACS Mater. Lett.*, 2023, **5**, 603-607.
13. X. Zhao, X. He, A. Hou, C. Cheng, X. Wang, Y. Yue, Z. Wu, H. Wu, B. Liu and H. Li, *Inorg. Chem.*, 2022, **61**, 9328-9338.
14. B. Tan, Z.-F. Wu and X.-Y. Huang, *Molecules*, 2022, **27**, 8789.
15. J. Espín, L. Garzón-Tovar, A. Carné-Sánchez, I. Imaz and D. Maspoch, *ACS Appl. Mater. Interfaces*, 2018, **10**, 9555-9562.
16. G. Chen, J. Sun, Q. Peng, Q. Sun, G. Wang, Y. Cai, X. Gu, Z. Shuai and B. Z. Tang, *Adv. Mater.*, 2020, **32**, 1908537.
17. S. Hussain, Z. Deng, A. Khan, P. Li, Z. Li, Z. Fang, X. Wan and X. Peng, *J. Membr. Sci.*, 2021, **620**, 118888.
18. L. Chen, D. Li, Y. Wang and C. Duan, *Nanoscale*, 2019, **11**, 11121-11127.
19. H. Ye, X. Li, L. Deng, P. Li, T. Zhang, X. Wang and B. S. Hsiao, *Ind. Eng. Chem. Res.*, 2019, **58**, 3269-3281.
20. D. Wang, X. Kan, C. Wu, Y. Gong, G. Guo, T. Liang, L. Wang, Z. Li and Y. Zhao, *Chem. Commun.*, 2020, **56**, 5223-5226.
21. Y. Shi, S. Liu, Z. Zhang, Y. Liu and M. Pang, *Chem. Commun.*, 2019, **55**, 14315-14318.
22. Z. Mi, P. Yang, R. Wang, J. Unruangsri, W. Yang, C. Wang and J. Guo, *J. Am. Chem. Soc.*, 2019, **141**, 14433-14442.
23. W. Hu, X. Miao, H. Tao, A. Baev, C. Ren, Q. Fan, T. He, W. Huang and P. N. Prasad, *ACS Nano*, 2019, **13**, 12006-12014.
24. J. Espín, L. Garzón-Tovar, G. Boix, I. Imaz and D. Maspoch, *Chem. Commun.*, 2018, **54**, 4184-4187.

25. T. Zhang, J.-W. Cao, X. Jiang, J. Chen, T. Wang and K.-J. Chen, *Crystal Growth Des.*, 2021, **21**, 729-734.
26. S. Tian, Z. Huang, J. Tan, X. Cui, Y. Xiao, Y. Wan, X. Li, Q. Zhao, S. Li and C.-S. Lee, *ACS Energy Lett.*, 2020, **5**, 2698-2705.
27. Y. Wang, W. Zhu, W. Du, X. Liu, X. Zhang, H. Dong and W. Hu, *Angew. Chem.*, Int. Ed., 2018, **130**, 4027-4031.
28. Z. He, L. Zhao, Q. Zhang, M. Chang, C. Li, H. Zhang, Y. Lu and Y. Chen, *Adv. Funct. Mater.*, 2020, **30**, 1910301.
29. J. Su, N. Xu, R. Murase, Z. M. Yang, D. M. D'Alessandro, J. L. Zuo and J. Zhu, *Angew. Chem.*, Int. Ed.2021, **133**, 4839-4845.
30. H.-C. Ma, C.-C. Zhao, G.-J. Chen and Y.-B. Dong, *Nat. Commun.*, 2019, **10**, 3368.
31. H. Li, H. Wen, Z. Zhang, N. Song, R. T. K. Kwok, J. W. Y. Lam, L. Wang, D. Wang and B. Z. Tang, *Angew. Chem. Int. Ed.*, 2020, **59**, 20371-20375.
32. Q. Ma, P. Yin, M. Zhao, Z. Luo, Y. Huang, Q. He, Y. Yu, Z. Liu, Z. Hu and B. Chen, *Adv. Mater.*, 2019, **31**, 1808249.
33. H.-C. Ma, G.-J. Chen, F. Huang and Y.-B. Dong, *J. Am. Chem. Soc.*, 2020, **142**, 12574-12578.
34. X. Ma, W. Fang, Y. Guo, Z. Li, D. Chen, W. Ying, Z. Xu, C. Gao and X. Peng, *Small*, 2019, **15**, 1900354.